

# Multiresonant luminophores based on the effect of thermally activated delayed fluorescence for the 3rd- and 4th-generation organic light-emitting diodes

© D.I. Dominskiy<sup>1,2</sup>, O.G. Kharlanov<sup>1</sup>, D.Yu. Paraschuk<sup>1,¶</sup>

<sup>1</sup> Department of Physics, Moscow State University, Moscow, Russia

<sup>2</sup> Enikolopov Institute of Synthetic Polymeric Materials, Russian Academy of Sciences, Moscow, Russia

¶e-mail: paras@physics.msu.ru

Received July 07, 2024

Revised July 07, 2024

Accepted July 29, 2024

We review the latest advances in the field of the most promising luminophores exhibiting the delayed fluorescence effect for organic light-emitting diodes, with a special focus on the so-called multiresonant luminophores, which are distinguished from other types of organic luminophores by their narrow emission bandwidth. A brief overview is given on the generations of organic light-emitting diodes, the principles of operation of multiresonant luminophores, features of their structure and their photophysical and luminescent properties are outlined. Advances and challenges in the field of multiresonant luminophores are analyzed and approaches to their molecular design are discussed.

**Keywords:** organic semiconductor, organic light-emitting diode, oled, thermally activated delayed fluorescence, TADF, fluorescence, multiresonant, external quantum efficiency.

DOI: 10.61011/EOS.2024.08.60031.6867-24

## Introduction

Organic light-emitting diodes (OLEDs) serve as one of the most promising types of light-emitting electronic devices due to low operating voltage, fast response, high brightness, and capability of achieving mechanical flexibility and/or semitransparency on flexible and/or transparent substrates. In recent decades, OLEDs serve as the basis of rapidly developing modern LED display technologies, gradually replacing traditional LCD technology. In the future, OLEDs may become light sources for lighting applications, including conformal ones with an arbitrary nonplanar surface and flexible sources. Moreover, the OLED's emitting area can be of almost any size, in sharp contrast with popular inorganic LEDs having a small emitting area.

LEDs are based on the electroluminescence (EL) effect, whose efficiency is defined by the rate of radiative recombination of electron-hole pairs injected from the LED electrodes. In organic materials, the lowest electronic excited states correspond to excitons, or, in terms of semiconductor physics, electron-hole pairs bound by coulombic attraction. Exciton binding energy in organic materials is considerably higher than the thermal energy at room temperature, which makes them the lowest excited states. Deep studies in exciton physics emerged in the 1960s: the first monograph in this field written by V.M. Agranovich — one of the pioneers in the exciton theory — was published in 1968 [1]. Excitons play a key role in OLEDs because their generation, transport, recombination processes and interaction with other quasiparticles are critical for the OLED efficiency.

Increase in the OLED efficiency and operational lifetime is the key objective in this field. Moreover, for display technology, it is important to achieve the highest possible EL color purity (i.e., monochromaticity) for each of the primary colors — red, green, and blue — to achieve fuller color reproduction. This paper reviews the recent achievements and issues in one of the most promising, fast-growing and young OLED fields that emerged in 2016 and is based on the so-called multiresonant (MR) luminophores [2]. Luminophores of this type potentially have a 100% fluorescence (FL) quantum yield (QY) and a narrow FL band compared with that of semiconductor quantum dots. This review mostly focuses on the concepts, approaches, and issues in the field of MR luminophores and to a lesser extent on MR luminophores themselves that are addressed in a series of recent works [3–5].

## OLED generations

The OLED light-emitting diodes layer includes organic luminophores with a triplet state ( $T_1$ ) whose energy is typically  $\Delta E_{ST} \sim 0.3\text{--}0.6$  eV below the first excited singlet state ( $S_1$ ), see Figure 1. One of the key factors affecting the OLED efficiency is the EL quantum yield, defined as the probability of emitting a photon per one electron-hole pair injected into OLED. Internal and external ELQYs are distinguished as follows: the first one describes the total number of EL photons emitted in the OLED active layer, while the second one is the number of EL photons that exited from OLED to the solid angle  $2\pi$  formed by the OLED emitting area. Whereas the internal ELQY may reach

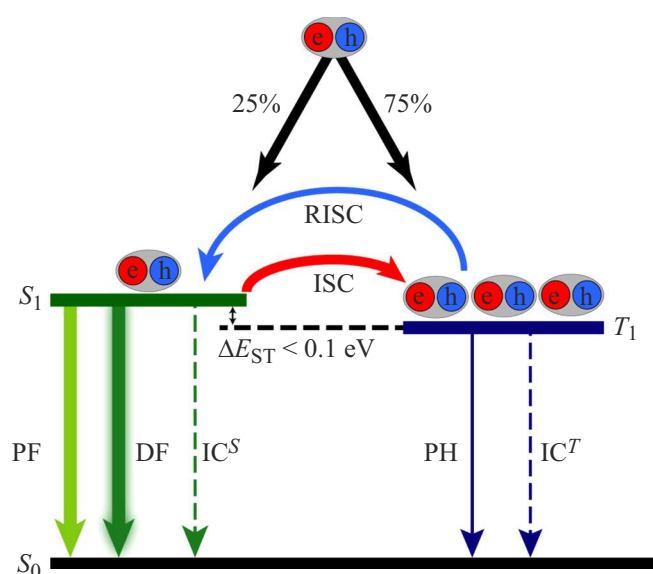


**Figure 1.** Jablonski diagram with the flowchart of main relaxation processes following electric excitation of a thermally delayed fluorescence (TADF) luminophore.  $S_0$  and  $S_1$  are the singlet ground and excited states,  $T_1$  is the triplet state,  $\Delta E_{ST}$  is the energy difference between the  $S_1$  and  $T_1$  states. PF is the prompt fluorescence, DF is the delayed fluorescence,  $IC^S$  and  $IC^T$  are the internal conversion, respectively,  $S_1 \rightarrow S_0$  and  $T_1 \rightarrow S_0$ , ISC is the intersystem crossing, RISC is the reverse intersystem crossing, PH is the phosphorescence.

100%, the external ELQY is always much lower due to a relatively low light outcoupling efficiency as a result of total internal EL reflection in the OLED layers and nonoptimal orientation of the EL emitting dipoles that, ideally, should be oriented in the OLED plane. Therefore, if no special measures for orientation of light-emitting diodes dipoles and reduction of waveguide-effect-related losses are taken in real practice, the external ELQY does not exceed 20–30% [6,7].

Generally (if no special spin-selective electrodes are used), due to the random spin statistics of electron-hole pairs injected from the electrodes, 75% of these pairs may generate triplet excitons. In turn, radiative transitions of triplet excitons to the ground state ( $S_0$ ) have extremely low rates, being forbidden in the dipole approximation; therefore, most organic luminophores usually relax nonradiatively from these states. First-generation OLEDs based on FL (i.e. on the  $S_1 \rightarrow S_0$  transition) lose as much as 75% in ELQY because its theoretical limit is 25%, which corresponds to the probability of singlet electron-hole pair formation assuming random spin statistics. The probability of radiative transition from the triplet state  $T_1$  to the ground state  $S_0$  ( $T_1 \rightarrow S_0$ ), i.e. phosphorescence, is considerably enhanced in the presence of heavy atoms (for example, iridium) in the luminophore; such molecules are the basis for the active layer of many commercial second-generation OLEDs (Figure 2). In principle, ELQY of OLEDs based on phosphors with heavy atoms may reach 100%, however,

they have a number of disadvantages. For example, it is not easy to fabricate stable blue and violet OLEDs probably due to a relative weakness of the corresponding metal-carbon bonds; moreover, the most successful iridium phosphorescent luminophores are rather expensive and have a relatively wide emission band, i.e. insufficient color purity, high degree of which is necessary for current and future display technologies. Difficulties in creating high-performance and long-lifetime blue luminophores for OLEDs have resulted in a situation where the blue pixel in modern three-color smartphone screens occupies more than 50% of the total area of all pixels (blue, green, red) to ensure the acceptable brightness [8], which, in particular, may limit the resolution of OLED-based screens.

Research community is currently focused on the third-generation OLEDs (Figure 2) that are based on luminophores exhibiting thermally assisted delayed fluorescence (TADF), see Figure 1. Such luminophores were known before, but the rapid development of TADF-based OLEDs was kickstarted by the work of Adachi *et al.* in 2012 [9] and has resulted in over 3,000 articles published on the TADF topic to date. In TADF luminophores, the  $S_1$  and  $T_1$  levels are so close in energy that there is a high probability of thermally assisted reverse intersystem crossing (RISC) from the triplet state to the singlet state ( $T_1 \rightarrow S_1$ ); fluorescent transition from the latter to the ground state ( $S_1 \rightarrow S_0$ ) occurs with a delay determined by the RISC rate. As in the 2nd-generation OLEDs, both triplet and singlet excitons contribute to EL, so ELQY of the 3rd-generation OLEDs can potentially reach 100%. For example, in 2023, achievement of a nearly-100% internal ELQY for a blue single-layer TADF OLED was reported [10]. The main objective of the molecular design of TADF molecules is to reduce  $\Delta E_{ST}$  down to a value of the order of thermal energy at room temperature (25 meV), meanwhile retaining a noticeable oscillator strength of  $S_1 \rightarrow S_0$  transition, to prevent competing nonradiative processes from deactivating the  $S_1$  and  $T_1$  states.

A concept of fourth-generation OLEDs is currently being formed to compensate for the disadvantages of TADF materials. For example, the most challenging bottleneck of TADF luminophores is a long fluorescence lifetime resulting from a small dipole moment of the  $S_1 \rightarrow S_0$  transition and/or from a relatively slow RISC process. The latter leads to an elevated concentration of triplet excitons in the OLED active layer and, thus, to a limitation of the OLED operational lifetime. Indeed, since the triplet exciton lifetime is relatively high, their elevated concentration leads to a higher probability of triplet-triplet, singlet-triplet and triplet-polaron annihilation. These processes, in turn, lead to considerable energy release, in particular, at host or dopant molecules of the OLED active layer, which increases the probability of various destructive processes such as dissociation of chemical bonds of the dopant and/or host molecules [11]. One can compensate these disadvantages of TADF materials within the so-called hyperfluorescence concept that is assigned to the 4th-generation OLED. The

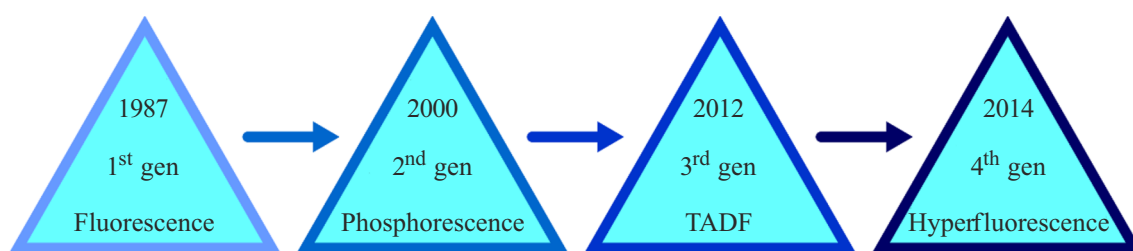


Figure 2. OLED generations.

approach is based on adding an extra, so-called terminal emitter to the OLED emitting layer already doped with the TADF luminophore. The terminal emitter accepts energy from the  $S_1$  state of the TADF luminophore through energy transfer [12]. Thus, in hyperfluorescent OLEDs, exciton generation, transport and radiative relaxation are performed by different materials. However, a complicated structure of the emitting layer is the reverse side of such separation of the functions by different materials, which may be an obstacle on the way to commercialization. Finally, one of the fascinating and counterintuitive ideas that should be assigned to the 4th-generation OLED approaches is the creation of luminophores with an inverse  $ST$ -gap ( $E(T_1) > E(S_1)$ ), which generally makes it possible to achieve a 100% FLQY/ELQY without TADF. Though this idea contradicts the simplest version of Hund's rule, it has been recently implemented experimentally by a Japanese research group [13]. So far, however, the inverse  $ST$ -gap has been experimentally confirmed only for a couple of *DABNA* derivatives [14] and one type of compounds with quite sophisticated synthesis [15], and molecular design approaches for such luminophores are in their infancy [16].

## Structure and properties of multiresonant luminophores

### TADF luminophores

A common feature of the molecular structure of TADF luminophores is the presence of donor and acceptor fragments. The highest occupied molecular orbital (HOMO) is localized mainly on the donor fragments and the lowest unoccupied molecular orbital (LUMO) is localized mainly on the acceptor fragments (Figure 3). As a result, the overlap of frontier orbitals (i.e. LUMO and HOMO) is relatively small, which makes it possible to reduce considerably the energy splitting of the  $S_1$  and  $T_1$  states ( $\Delta E_{ST}$ ) and to ensure an efficient delayed FL.

The most studied TADF luminophores consisting of at least one donor and one acceptor molecular fragments are known as donor-acceptor luminophores. Among the donor fragments of TADF luminophores, carbazole, spiro-acridine, triphenylamine, and their derivatives are most widely used. Benzonitrile, triazine, diphenylsulfone, benzophenone, and their derivatives are generally used as acceptor fragments.

Small frontier-orbital overlap is often achieved by rotating the molecule's acceptor fragments with respect to the donor ones (both of them are usually planar) at a relatively large angle to considerably reduce overlap of the  $\pi$ -orbitals of the specified fragments. A less often used concept of charge-transfer donor-acceptor complexes relates to the case of the approximately parallel donor and acceptor fragments interacting mainly „through space“ [17–23], i.e. similar to the interaction between the donor and acceptor molecules in charge-transfer intermolecular complexes. However, small frontier-orbital overlaps in such donor-acceptor TADF luminophores usually lead to a low oscillator strength of the  $S_0$ – $S_1$  transition, which considerably increases the luminophore's radiative relaxation time allowing various nonradiative processes to deactivate the  $S_1$  state and, thus, to reduce the luminescence QY. Thus, the low oscillator strength of the  $S_1$ – $S_0$  transition, which is a significant disadvantage of the donor-acceptor TADF luminophores, is often the price one has to pay for a small  $\Delta E_{ST}$  splitting.

A wide emission band (more than 50 nm at half maximum) is another significant disadvantage of the donor-acceptor TADF luminophores, which considerably reduces the color purity, a critical property for current and future display technologies. To overcome the above-mentioned disadvantages, in 2015–2016, a Japanese group led by T. Hatakeyama proposed a new type of TADF luminophores known as multiresonant luminophores [2,24], where the spatial separation of frontier molecular orbitals is implemented at the alternating donor and acceptor atoms, rather than at polyatomic donor and acceptor molecular fragments<sup>1</sup> [2]. MR molecules are polycyclic hydrocarbons with acceptor and donor heteroatoms, for example, boron and nitrogen, respectively, which correspond to ortho-substituents on the benzene ring (D and A with respect to three external benzene rings in Figure 3, *b*). In the structure of the MR molecule, the donor and acceptor atoms themselves are located in a para position with respect to each other. Such structure leads to localization of the HOMO/LUMO mainly at the donor/acceptor atoms and carbon atoms that are in meta positions with respect to these atoms. In alternant

<sup>1</sup> The term „multiresonant“ appeals to the so-called resonance theory proposed by L. Pauling, which was an intuitive evolution of the valence bond method. The presence of donor and acceptor atoms in the above-mentioned positions on aromatic rings lets one draw many various resonant structures within the resonance theory.

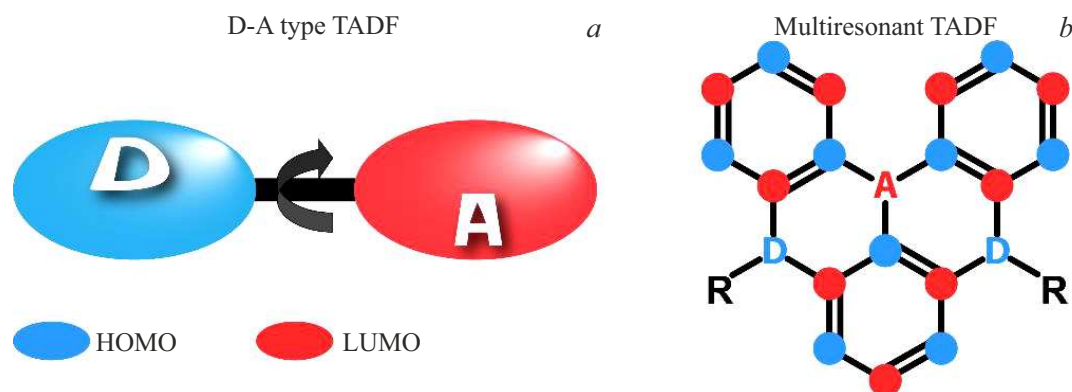


**Figure 3.** Illustration of molecular design concepts for TADF luminophores. (a) Donor-acceptor TADF luminophores usually contain covalent-bonded donor and acceptor molecular fragments that are usually rotated from each other at a significant angle to reduce the HOMO/LUMO overlap. (b) In MRTADF luminophores, electron-donor atoms are placed in ortho positions on the conjugated ring with respect to electron-acceptor atoms in the annulated aromatic structure, resulting in the HOMO/LUMO localization mainly on donor/acceptor atoms.

hydrocarbons, which MR luminophores are usually assigned to, all atoms can be classified into two groups — the „blue“ and the „red“ ones in Figure 3, *b* (also referred to as marked and unmarked [25]), — so that blue/red atoms are bonded only to red/blue atoms, respectively. As a result, one frontier orbital (HOMO) in MR luminophores is localized mainly at the blue atoms and the other one (LUMO) is localized mainly at the red atoms (Figure 3, *b*).

In comparison with the donor-acceptor TADF luminophores having a wide emission band, MR luminophores generally demonstrate a narrow band [5]: typical FL bandwidths are 20–40 nm [26–28] and down to 14 nm in record-breaking cases [26] (Figure 4). This is achieved due to the two following circumstances. First, frontier molecular orbitals in MR luminophores are non-bonding in the ideal case [25] because they vanish at the nearest neighbors of a given atom, i.e. between the nearest pairs of blue (red) atoms in Figure 3, *b*. As a result, the electron density between these neighboring atoms, which is defined by the frontier orbitals, vanishes. Consequently, the order of the corresponding  $\pi$ -bonds is equal to zero [29], because the ground-state electron density is mainly localized at the group of blue (red) atoms. Therefore, bond length variation, in particular, due to vibrations, does not affect the frontier orbital energies and their contributions to the electron-vibronic (vibronic) interaction. Such an alternant feature of the frontier orbital topology leads to a strongly suppressed vibrational structure of absorption and emission bands of the MR molecules and, thus, can provide a narrow emission bandwidth. Second, a rigid molecular structure of the MR luminophore makes it possible to get rid of typical low-frequency vibrational modes that are typical of the donor-acceptor TADF luminophores. As a matter of fact, the donor and acceptor fragments are often connected by one covalent (usually single) bond, around which low-frequency vibrations are possible that strongly modulate the overlap of frontier orbitals and, thus, provide a strong

vibronic coupling. In turn, the strong coupling leads to high Huang–Rhys factors and, therefore, to wide absorption and luminescence spectra. Similar low-frequency vibrations are possible in the case of „through-space“ interaction between the donor and acceptor molecular fragments.

A common feature of the donor-acceptor TADF luminophores is the low oscillator strength of the  $S_1$ – $S_0$  transition as a result of small overlaps of their frontier orbitals — HOMO and LUMO. However, because of multiple, but relatively small overlap „patches“ of frontier orbitals in the MR luminophores, the oscillator strength of the  $S_0$ – $S_1$  transition can be quite high for them. For example, for the very first MR luminophores, it was in the range of 0.2–0.4 [2,5], for other luminophores, the oscillator strength reached 0.7 [30]. As a result of the considerable oscillator strength of the  $S_0$ – $S_1$  transition and the weak vibronic coupling that facilitates reduction of the nonradiative relaxation efficiency, FLQY of the MR luminophores can reach 90% and higher [2,5]. Note that, owing to the above-mentioned multiple overlap patches of frontier orbitals, reduction of the electron repulsion effects should be expected, which should facilitate reduction of  $\Delta E_{ST}$  compared with the donor-acceptor TADF luminophores.

The most pronounced alternant topology of the frontier orbitals is implemented when a series of marked and unmarked atoms in the polycyclic skeleton of the MR luminophores are substituted with atoms having strong acceptor and donor properties, i.e. with boron and nitrogen, respectively. Thus, for example, by varying the degree of substitution of carbon atoms in graphene with nitrogen and boron atoms, the band gap of the material can be changed from zero (graphene, no heteroatoms), to  $\sim 6$  eV (hexagonal boron nitride) [31], no carbon atoms, with the HOMO localized at nitrogen atoms [32]).

Besides boron, the acceptor atom can be carbon from the carbonyl group ( $>C=O$ ) whose bivalent nature governs its location only at the periphery of a polycyclic MR

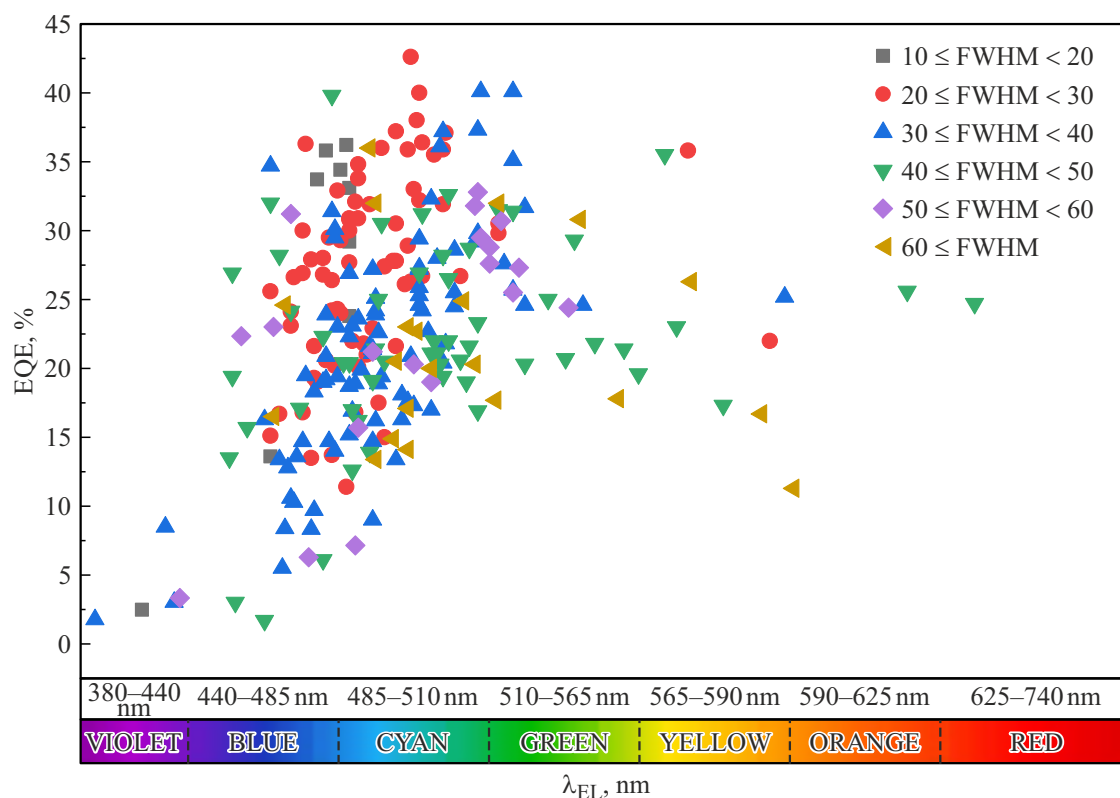


**Figure 4.** External quantum efficiency, EQE, of OLEDs with active layer based on MR luminophores for various EL wavelengths,  $\lambda_{EL}$  [4,41-92]. Full width at half maximum (FWHM) is given in nanometers.

luminophore (*QAD-2Cz*, Figure 5). Besides nitrogen, the donor atom can be oxygen from an ether group (*PXZ-BN*, Figure 5), as well as other elements from the chalcogen group, for example, sulfur (*2PTZBN*, Figure 5) and selenium (*CzBSe*, Figure 5). Inclusion of atoms (into the respective positions, see Figure 3, *b*) with stronger donor properties or with more pronounced acceptor properties into the molecular structure of the MRTADF luminophores leads to an increase in the HOMO energy and to a decrease in the LUMO energy, respectively. Thus, the optical gap of an MR luminophore can be adjusted. MR luminophores are sometimes classified into the following groups in accordance with the types of electron-acceptor and electron-donor atoms included in them: boron/nitrogen (B/N) [2,33], boron/oxygen (B/O) [26,34], carbonyl/nitrogen ( $>C=O/N$ ) [35,36], [35,36], so-called multi-heteroatomic systems, where more than two different types of heteroatoms are used [27,37], and novel indolocarbazole-based  $\pi$ -systems (*t3IDCz*, Figure 5) [38,39] that do not contain apparent acceptor heteroatoms. Note that not all MR luminophores exhibit the TADF effect as, for example, indolocarbazole luminophores [40]. This is probably associated with too large a  $\Delta E_{ST}$  gap of about 0.3 eV [40] which is accounted for by the large frontier-orbital overlaps in them, larger than those in the donor-acceptor MRTADF luminophores.

As for the field of inorganic LEDs, the key objective is to develop an efficient, bright and durable OLED that emits blue and violet narrow-band EL because all other spectral colors can be relatively easily generated from such short-wavelength radiation using appropriate luminophores. Figure 4 shows the values of external ELQY reported in published studies for most of the known MR luminophores emitting in various spectral ranges. As shown in the figure, most of the research is devoted to blue luminophores for which external ELQY of up to 40% is reported. Not too many MR luminophores have a narrow EL bandwidth, and this is a sign of insufficient level of understanding of the correlation between the molecular structure and the luminescence bandwidth.

MR luminophores from the B/N group (Figure 5) are the most well-studied ones. For this group, the first MRTADF luminophore called *DABNA* (*5,9-diphenyl-5,9-diaza-13b-boranaphtho[3,2,1-de]anthracene*), as well as *DABNA-1* and several derivatives thereof were synthesized [2,26,93,94]. There are over 1200 citations of one of the first reports on *DABNA*-type luminophores published in 2016 [2]. Just over 10 research teams primarily from Southeast Asia, in particular, China and Japan, are currently working in the field of *DABNA*-type luminophores. *DABNA-1* and *DABNA-2* luminophores have demonstrated violet and blue (400–469 nm) radiation with FLQY of 88% and 90%, respectively, at  $\Delta E_{ST}$  of 0.18 eV and 0.15 eV in a

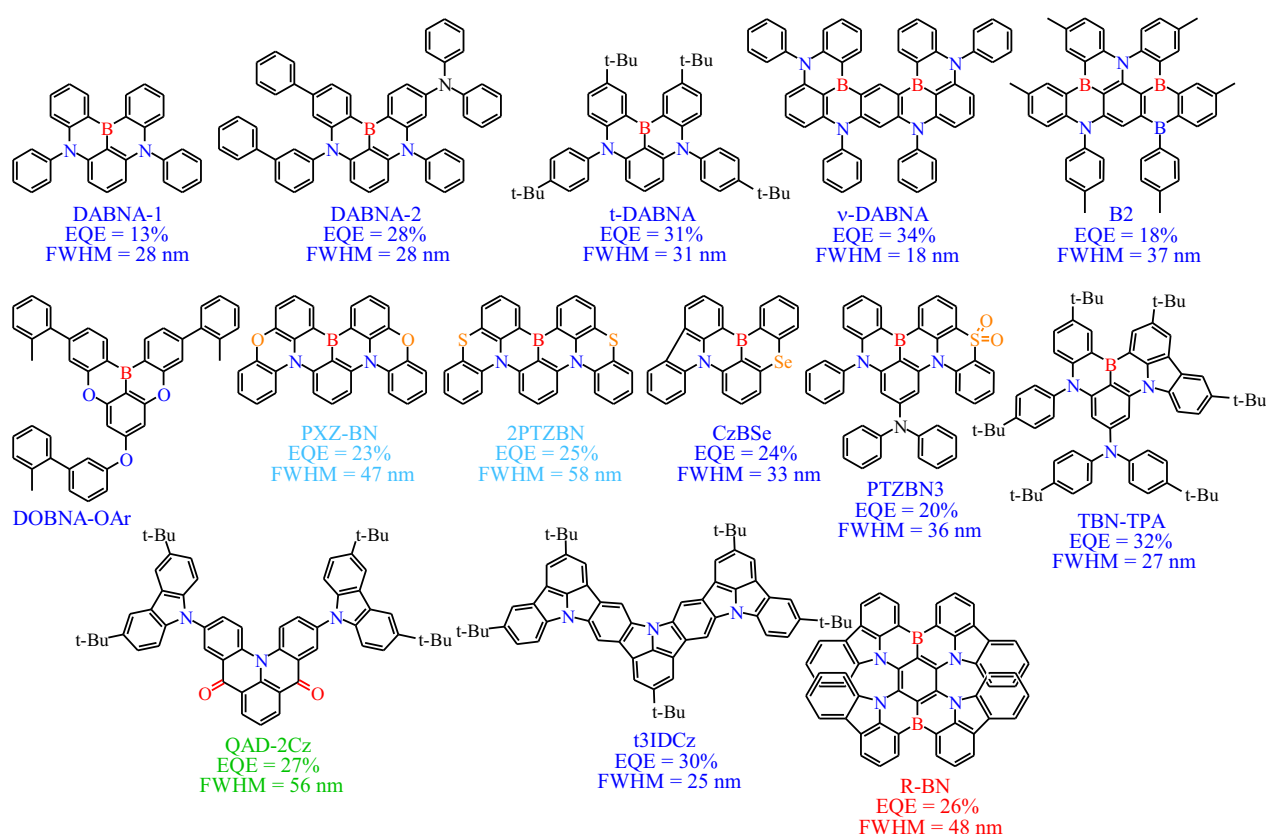


**Figure 5.** Examples of MRTADF luminophores. Color of each name corresponds to the luminescence spectrum [4].

well-known *mCBP* film (with a doping level of 1 wt.%) that is widely used as a host for luminophores in various types of OLEDs. These films as part of the OLED active layer have shown high ELQY of 13.5% and 20.2% with violet color coordinates (0.13, 0.09) and (0.12, 0.13), respectively, along with narrow EL spectra (FWHM of 28 nm). Though OLEDs based on *DABNA-1* and *DABNA-2* have shown very high roll-off with an increase in the OLED current value, they are promising candidates for the development of pure violet TADF materials.

A *DABNA-1* derivative known as *t-DABNA* [33] is another prominent representative of the boron-nitrogen MR luminophore group. The authors reported that *t-DABNA*-based OLED samples had the maximum ELQY of 31%. In another study, addition of carbazole to the boron atom in para position in the *t-DABNA* structure (*TBN-TPA*) increased FLQY to 97% and reduced  $\Delta E_{ST}$  to 0.03 eV in a toluene solution [95]. A *TBN-TPA*-based blue OLED has shown a very high external ELQY of 32% with its peak at 447 nm and FWHM of 27 nm [95]. In 2018, *DABNA* derivatives with two and three boron atoms (*B1-4*) were demonstrated [96]. All the materials showed violet and blue emission in the range from 441 nm to 455 nm with FWHM of 32–34 nm in *PMMA* films with the doping level of 1 wt.%. FLQY was within 33–57%, and  $\Delta E_{ST}$  was within 0.15–0.18 eV in the *PMMA* films. OLEDs with one of the synthesized materials (*B2*, Figure 5)

in a concentration of 1 wt.% in the *mCBP* host have demonstrated a maximum external ELQY of 18% with an EL peak at 460 nm and FWHM of 37 nm. A *DABNA-1* core dimer (*v-DABNA*) with two boron atoms and two donor groups based on diphenylamine attached to the *DABNA* cores in para positions with respect to the boron atom was reported in 2019 (Figure 5) [26]. *v-DABNA* luminophore in the *DOBNA-OAr* host (1 wt.%) has shown FLQY of 90% with its peak at 467 nm and  $\Delta E_{ST} = 17$  meV. Though the  $\pi$ -conjugation degree of *v-DABNA* has increased compared with *DABNA-1*, the emission peak was still in the blue region as for *DABNA-1*. This can probably be attributed to a somewhat nonplanar conformation of the polycyclic molecule skeleton leading to reduction of the characteristic delocalization length of the  $\pi$ -electrons and not causing optical gap reduction. However, compared with *DABNA-1*, *v-DABNA* has increased FLQY and reduced  $\Delta E_{ST}$ . A *v-DABNA*-based OLED has shown a record-breaking external ELQY (34.4%) with blue color coordinates (0.12, 0.11) and very narrow EL width (18 nm at half maximum) [26]. Moreover, this device has shown quite a low efficiency roll-off with brightness, below 10% at 1000 cd/m<sup>2</sup>. This is currently the highest efficiency and lowest roll-off among OLEDs based on the MRTADF luminophores. Though most of the studies on MR luminophores are focused on the blue spectrum, attempts were made to achieve green-emitting and red-emitting luminophores. For exam-

ple, the *QAD-2Cz* compound using a carbonyl/nitrogen donor-acceptor pair has shown an emission wavelength of 530 nm with a maximum ELQY of 27% at a sufficiently high  $\Delta E_{ST} = 170$  meV [97]. *R-BN* MR luminophore and its derivative with red-emitting tertiary-butyl substituents *R-TBN* were demonstrated in [98]. The authors claimed to have created OLEDs based on MRTADF luminophores with the longest wavelength, with EL spectra peaks at 664 nm and 686 nm at ELQY up to 28%.

Note that relatively planar MR luminophores are prone to aggregation with formation of H-aggregates, which feature a low oscillator strength of the  $S_0-S_1$  transition, so that the luminescence efficiency may be reduced. To inhibit the aggregation effects in MR luminophores, bulky alkyl (methyls, tertiary butyls) or  $\pi$ -conjugated (phenyl, carbazole, etc.) substituents are added to their molecular structure. One typically attempts to arrange substituents of the latter type at a large angle (usually more than  $60^\circ$ ) to the plane of the  $\pi$ -conjugated molecular core typically by using steric effects. Moreover, molecular orbitals of the  $\pi$ -conjugated substituents, even when oriented at a large angle, can partially overlap with those of the  $\pi$ -conjugated core of the MR luminophore, which is used to shift the emission spectrum into a longer-wavelength region.

## RISC rate

One of the main disadvantages of all types of TADF luminophores is a relatively low RISC rate, which, first, may reduce the TADF efficiency and, second, leads to a relatively high concentration of triplet excitons. The latter ones have a long lifetime and, as mentioned above, serve as precursors for various OLED degradation processes. Therefore, in terms of molecular design of the MRTADF luminophores, the research community is focused to a great extent on the increase in the RISC rate (Figure 1) characterized by the rate constant  $k_{RISC}$ .

RISC is a nonradiative transition induced by spin-orbit coupling with the corresponding matrix element  $\langle S_1 | \hat{H}_{SO} | T_1 \rangle$  for two electron states  $|S_1\rangle$  and  $|T_1\rangle$ , where  $\hat{H}_{SO}$  is the spin-orbit coupling operator, so that  $k_{RISC} \propto |\langle S_1 | \hat{H}_{SO} | T_1 \rangle|^2$ , according to the Fermi golden rule. Within the most popular approach,  $k_{RISC}$  is calculated using the semiclassical Marcus theory (Marcus–Levich–Jortner model) [99,100]:

$$k_{RISC} = \frac{2\pi}{\hbar} |\langle S_1 | \hat{H}_{SO} | T_1 \rangle|^2 \times \text{FCWD}, \quad (1)$$

where  $\hbar$  is the reduced Planck's constant, and FCWD is the Franck–Condon weighted density of states calculated from the vibrational spectrum of  $|T_1\rangle$ . Note that FCWD contains an exponential factor whose exponent includes  $\Delta E_{ST}$ , due to which  $k_{RISC}$  grows significantly as  $\Delta E_{ST}$  reduces.

## Matrix element of the spin-orbit coupling operator

The spin-orbit coupling operator in the central-field approximation, which is deemed to be reasonable for many organic molecules, reads

$$\hat{H}_{SO} = \frac{e^2}{2m_e^2 c^2} \sum_I \sum_i \frac{Z_I^{\text{eff}}}{r_{iI}^3} \hat{\mathbf{l}}_{iI} \cdot \hat{\mathbf{s}}_i \quad (2)$$

where  $m_e$  is the electron mass,  $e$  is the electron charge,  $c$  is the speed of light,  $Z_I^{\text{eff}}$  is the effective dimensionless charge of nucleus  $I$ ,  $r_{iI}$  is the distance between the valence electron  $i$  and the nucleus  $I$ ,  $\hat{\mathbf{l}}_{iI}$  is the orbital momentum operator of the electron  $i$  with respect to the nucleus  $I$ ,  $\hat{\mathbf{s}}_i$  is the spin operator of the electron  $i$ .

As long as expression (2) corresponds to a fixed nuclear configuration, the matrix element  $\langle S_1 | \hat{H}_{SO} | T_1 \rangle$  in general depends on the coordinates of the nuclei  $Q$  and in the two-level model approximation can be written as:

$$\langle S_1 | \hat{H}_{SO} | T_1 \rangle = \langle S_1 | \hat{H}_{SO} | T_1 \rangle \Big|_{Q=0} + \sum_k \frac{\partial \langle S_1 | \hat{H}_{SO} | T_1 \rangle}{\partial Q_k} \Big|_{Q=0} \cdot Q_k, \quad (3)$$

where  $Q_k$  is the vibrational coordinate corresponding to the normal mode  $k$ , and the configuration  $Q = 0$  corresponds to some fixed position of the nuclei, for example, to the equilibrium geometry of  $|T_1\rangle$ . The first term in (3) corresponds to the Condon approximation on the basis of which equation (1) is derived, and the second term constitutes the Herzberg–Teller approximation. These Condon and Herzberg–Teller contributions are similar to those arising in the theory of optical transitions, where the operator of electric dipole interaction with electromagnetic radiation is used instead of  $\hat{H}_{SO}$ . At the same time, for some MRTADF luminophores, equation (3), whose second term includes the vibronic coupling, is still insufficient for a correct description of the spin-orbit coupling in them because higher-energy singlet and triplet states beyond  $S_1$  and  $T_1$  should be accounted for [101], i.e. it is necessary to go beyond the two-level model, see, for example, [30,102]. Such high-energy states can be considered in  $\langle S_1 | \hat{H}_{SO} | T_1 \rangle$  by including the spin-vibronic coupling, so that the second-order perturbation theory introduces mixing of electron states with the same multiplicity via the nuclear kinetic energy operator [101].

Namely, for example, in the  $\nu$ -*DABNA*-type luminophores and their analogues *BOBO-Z*, *BOBS-Z*, *BSBS-Z* containing the same polycyclic  $\pi$ -conjugated skeleton, but with the N atoms substituted with the O and/or S atoms, the experimental data on  $k_{RISC}$  agrees best with the theoretical data when both the Condon and Herzberg–Teller contributions according to equation (3), as well as the spin-vibronic contribution are considered in  $\langle S_1 | \hat{H}_{SO} | T_1 \rangle$  [102]. In particular, theoretical calculations performed by the authors show that, for  $\nu$ -*DABNA*, more than 80% of the contribution to  $\langle S_1 | \hat{H}_{SO} | T_1 \rangle$  is provided by the  $T_1 \rightarrow T_2 \rightarrow S_1$  transition induced by the spin-vibronic coupling, while

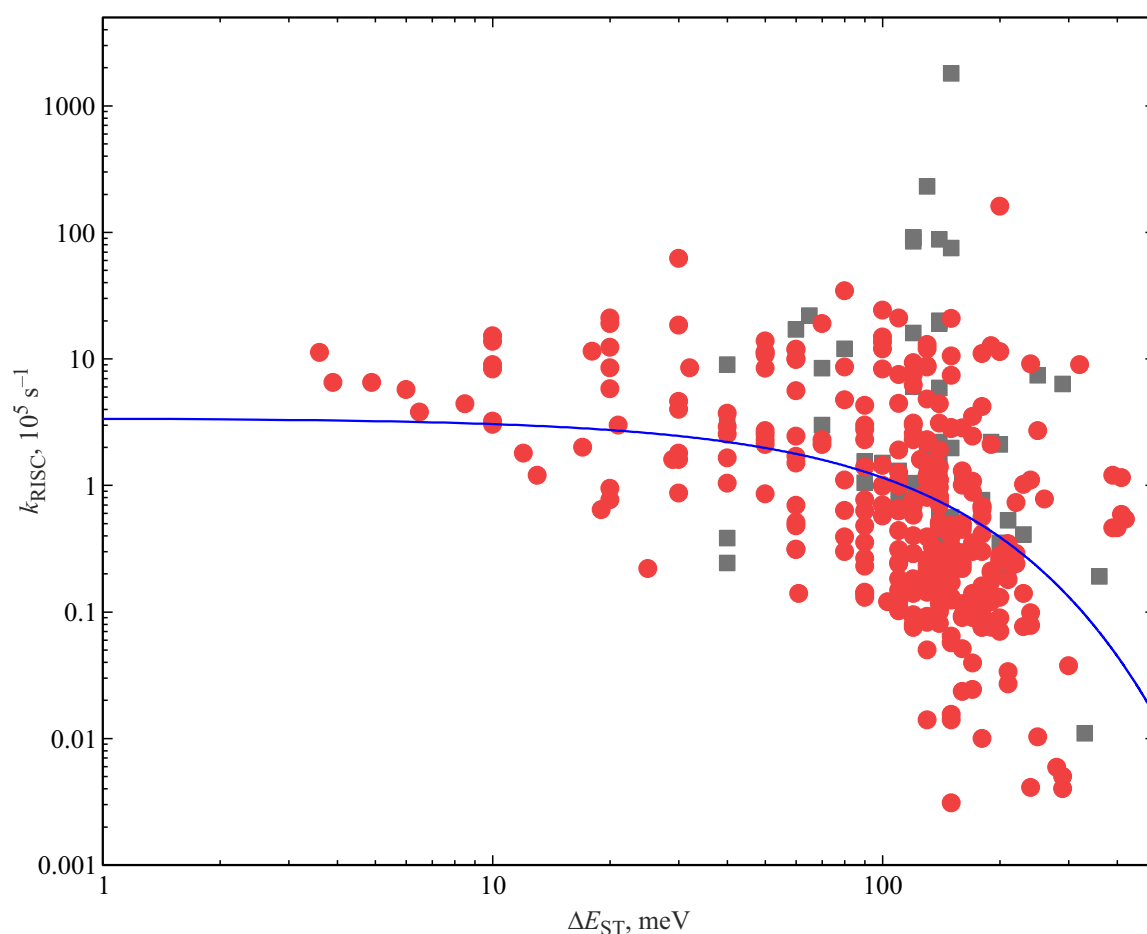


**Figure 6.** Correlation between the experimental  $k_{\text{RISC}}$  and  $\Delta E_{\text{ST}}$  value for the MR luminophores as reported in Refs. [5,55,61,64,69,72,79,81–92,121,122]. Smooth line corresponds to a linear regression in the  $(\log k_{\text{RISC}}, \Delta E_{\text{ST}})$  coordinates, with the Pearson correlation coefficient of  $-0.39$  and the  $p$ -value for  $t$ -test equal to  $7 \times 10^{-15}$ . Black dots indicate the MR luminophores containing one or more heavy atoms of the third and the following periods.

in luminophores with sulfur atoms (*BOBS-Z*, *BSBS-Z*), 97–98% of the contribution to  $\langle S_1 | \hat{H}_{\text{SO}} | T_1 \rangle$  is provided by the two-level model describing the  $T_1 \rightarrow S_1$  transition.

A much stronger spin-orbit coupling directly between  $|S_1\rangle$  and  $|T_1\rangle$  and a high  $k_{\text{RISC}}$  in *BOBS-Z* and *BSBS-Z* containing, respectively, one and two S atoms, as compared with  *$\nu$ -DABNA* and *BOBO-Z* [102] is associated with the heavy-atom (sulfur) effect. Indeed, spin-orbit coupling grows dramatically as the nuclear charge increases [103,104], which is known as the heavy atom effect. Therefore, inclusion of heavy atoms, in particular, of sulfur and heavier atoms, in the MRTADF luminophore structures should increase the RISC rate considerably, i.e. increase  $k_{\text{RISC}}$ , which is observed experimentally (see Figure 6, black dots). Thus, increase in the concentration of heavy atoms in the luminophore molecular structure might seem to be a good strategy for molecular design of the MRTADF luminophores. However, this approach may lead to a decrease in the OLED operational lifetime because heavy atoms form weaker chemical bonds, i.e. bonds having a relatively low bond dissociation energy compared with that for the C–C

bond. This weak-bond effect is particularly troublesome for blue iridium luminophores, for which, despite very high efforts, an acceptable stability for utilization in LED technologies has not been achieved.

Within the leading-order perturbative description of the spin-orbit coupling between the  $S_1$  and  $T_1$  states, the coordinate parts of wave functions of the two states correspond to the same electronic configuration with one electron on HOMO and one electron on LUMO. In the leading-order approximation, they can be constructed from the products of wave functions of these two orbitals,  $(\psi_{\text{HOMO}}(\mathbf{x}_1)\psi_{\text{LUMO}}(\mathbf{x}_2) \mp \psi_{\text{HOMO}}(\mathbf{x}_2)\psi_{\text{LUMO}}(\mathbf{x}_1))/\sqrt{2}$ , where the plus sign corresponds to  $S_1$ , the minus sign to  $T_1$ , and  $\mathbf{x}_{1,2}$  are the spatial coordinates of the electron pair that occupies HOMO and LUMO. As a result, in a planar molecule, for example,  $S_1$  and  $T_1$  have the same reflection properties with respect to the molecular plane, therefore, the Condon contribution to  $\langle S_1 | \hat{H}_{\text{SO}} | T_1 \rangle$  (first term in equation (3)) is suppressed. This selection rule is reflected in the El-Sayed rules [105], according to which the rate of ISC between the states corresponding to the

molecular orbitals of the same type (for example,  $S_1 \rightarrow T_1$ ) is much lower than that between the states with orbitals of different types (for example,  $S_1 \rightarrow T_2$ )<sup>2</sup>.

Moreover, the molecular point symmetry group can impose additional restrictions on  $\langle S_1 | \hat{H}_{SO} | T_1 \rangle$  [104,106]. Namely, selection rules associated with the symmetries of the molecule are governed by the orbital part  $\hat{H}_{SO}$  in equation (2) because spin degrees of freedom are internal and the unperturbed Hamiltonian without the spin-orbit coupling does not couple to them. In particular, in planar  $\pi$ -conjugated hydrocarbons where only atomic  $p_z$ -orbitals contribute to the frontier molecular orbitals, the purely electronic contribution to  $\langle S_1 | \hat{H}_{SO} | T_1 \rangle$ , i.e. one without considering the vibronic or spin-vibronic couplings (see equation (3)), is very small [103,104]. Indeed, the orbital momentum operator  $\hat{L}_I$  entering the Hamiltonian (2), when acting on the  $p_z$ -orbital of its own atom  $I$ , gives  $\hat{L}_{I,z} |p_{z,I}\rangle = 0$ , while the action of  $\hat{L}_{I,y}$  ( $\hat{L}_{I,x}$ ) is reduced to a rotation of the  $p_z$ -orbital by  $\pi/2$  about the  $y$  ( $x$ ) axis, i.e. to its transformation into a  $p_x$  ( $p_y$ ) orbital and multiplication by  $i\hbar$  ( $-i\hbar$ ) [103,104], or, in the general case,

$$\hat{L}_{I,\alpha} |p_{\beta,I}\rangle = i\hbar e_{\alpha\beta\gamma} |p_{\gamma,I}\rangle, \quad (4)$$

where indices  $\alpha, \beta, \gamma$  run over  $x, y, z$ , and  $e_{\alpha\beta\gamma}$  is the Levi-Civita symbol (totally antisymmetric unit pseudotensor). The matrix elements of  $\hat{L}_I$  follow from equation (4):  $\langle p_{\alpha,I} | \hat{L}_{I,\beta} | p_{\gamma,I} \rangle = i\hbar e_{\alpha\beta\gamma}$ . In particular, all diagonal matrix elements are equal to zero,  $\langle p_{z,I} | \hat{L}_I | p_{z,I} \rangle = 0$ , moreover, the matrix elements  $\langle p_{z,I} | r_I^{-3} \hat{L}_I | p_{z,I} \rangle$  are also vanish, where  $r_I$  is the distance from the electron to the  $I$ th nucleus. Figuratively speaking, interaction between the orbital motion of the  $p_z$ -electron and its spin vanishes. More rigorously, the matrix element  $\hat{H}_{SO}$  between the  $S_1$  and  $T_1$  states with the same electronic configuration reduces to single-electron spinless expectation values  $\langle \psi_{HOMO} | r_I^{-3} \hat{L}_{I,z} | \psi_{HOMO} \rangle$ ,  $\langle \psi_{LUMO} | r_I^{-3} \hat{L}_{I,z} | \psi_{LUMO} \rangle$  over the states that are linear combinations of atomic orbitals  $|p_{z,J}\rangle$ , and one-center contributions, that correspond to  $I = J$  in the sums over the latter ones, vanish. Thus, effectively, the  $S_1 \rightarrow T_1$  transition does not involve electron spin interactions with the intraatomic orbital momentum, but involves interactions only with the orbital momentum of the electron motion across the molecule, which is suppressed proportionally to the small atomic-orbital overlaps  $\langle p_{z,J} | p_{z,J'} \rangle$ ,  $J \neq J'$  [103,104]. In fact, the contributions to the interaction are made only by three-center integrals  $\langle p_{z,J} | r_I^{-3} \hat{L}_{I,z} | p_{z,J'} \rangle$ , i.e. by those with  $I \neq J \neq J' \neq I$ . It is important to note that the three-center integral values are considerably suppressed due to the  $r_I^{-3}$ , factor, which

<sup>2</sup> In this context, it is sometimes said that, according to the El-Sayed rules, a spin change from 0 to 1 during ISC should be accompanied by a change in the orbital momentum of the corresponding states. Such terminology is avoided here because  $S_1$  and  $T_1$ , generally speaking, do not have a definite orbital momentum (though being eigenfunctions of the reflection operator with respect to the molecular plane for planar molecules).

leads to an extremely weak spin-orbit coupling in planar  $\pi$ -conjugated hydrocarbons [103].

Nevertheless, the polycyclic skeleton of the MR luminophores often contains the N atoms (see, for example, Figure 5) that are not in the pure  $sp^2$ -hybridized state, but host a minor contribution of the  $sp^3$ -hybridized orbitals resulting in the N atoms being slightly out of the molecular plane, the molecule thus becoming non-planar. As a result of such a symmetry breaking, the  $\pi$ -orbitals have a small admixture of the  $\sigma$ -orbitals, so that the  $\pi$ -orbitals include not only the  $p_z$ -components of atomic orbitals, but also low-weight  $p_x$ - and  $p_y$ -components. Hence, a contribution to the matrix element  $\hat{H}_{SO}$  can now be made by the nonzero matrix elements of  $\hat{L}_I$  corresponding to the same atom (see equation (4)), for example,  $\langle p_{x,I} | r_I^{-3} \hat{L}_{I,y} | p_{z,I} \rangle$ , so the spin-orbit coupling may be considerably enhanced compared with the planar-molecule case [107,108]. Thus, nitrogen atoms included in the polycyclic structure of the MR luminophore, should contribute to increasing  $k_{RISC}$ . In addition, lone electron pairs of the  $n$ -orbitals of the nitrogen atoms (as well as, for example, those of oxygen and sulfur atoms) can also actively contribute to the spin-orbit coupling, due to the following factors. First, the corresponding  $n\pi$ -transitions may contribute significantly to the excited states of various multiplicities. Second, the  $n$ -orbitals are oriented in the plane of the  $\pi$ -conjugated molecule, i.e. perpendicularly to the  $p_z$ -orbitals, which ensures a considerable magnitude of the  $\langle n_I | r_I^{-3} \hat{L}_{I,y} | p_{z,I} \rangle$  matrix element (see equation (4), where  $I$  corresponds to the N atom) because the rotated  $p_z$ -orbital corresponding to  $\hat{L}_{I,y} | p_{z,I} \rangle$  significantly overlaps with the  $n$ -orbital [104,106]. As a result, the singlet-triplet transition matrix elements between the  $\pi\pi$ - and  $n\pi^*$ -states,  $\langle S_{\pi\pi^*} | \hat{H}_{SO} | T_{n\pi^*} \rangle$ , can be much larger than the matrix elements that connect the states formed only by the  $\pi$ -electrons,  $\langle S_{\pi\pi^*} | \hat{H}_{SO} | T_{\pi\pi^*} \rangle$ , in accordance with the El-Sayed rules [104,105,108]. In polyheterocyclic compounds, the  $n\pi^*$ -transitions are supposed to contribute significantly to higher states, in particular, to  $S_2$  and  $T_2$ , and may contribute considerably to ISC and RISC [104,106]. At the same time, according to the quantum chemical calculations within the two-level model, for the MR-TADF luminophores without heavy atoms, typical matrix elements of the spin-orbit coupling are not too high for  $\langle S_1 | \hat{H}_{SO} | T_1 \rangle$  ( $\sim 0.01 \text{ cm}^{-1}$ ), but are much higher for  $\langle S_1 | \hat{H}_{SO} | T_n \rangle$  ( $\sim 0.5 \text{ cm}^{-1}$ ,  $n = 2, 3$ ) [30,82], which agrees with the El-Sayed rules. Note that the typical values of  $\langle S_1 | \hat{H}_{SO} | T_1 \rangle$  for iridium phosphors used in the 2nd-generation OLEDs are 2 to 3 orders of magnitude higher and exceed  $100 \text{ cm}^{-1}$  [99].

### RISC rate constant: experimental approaches

In a number of cases,  $k_{RISC}$  can be extracted from the experimental FL kinetics and FLQY  $\Phi = \Phi_p + \Phi_d$ , where „p“ and „d“ subscripts refer to the prompt and delayed FL, respectively, using a three-level kinetic model describing

the photophysical processes shown in Figure 1 [109]. FL kinetics of the TADF luminophores usually has a typical two-exponential profile with decay times  $\tau_p$  and  $\tau_d$  corresponding to the prompt and delayed FL (PF and DF in Figure 1), respectively. As long as  $\tau_p$  and  $\tau_d$  are usually in the nanosecond and microsecond range, respectively, (sometimes in submillisecond range [110]),  $\Phi_d/\Phi_p$  can be extracted from the experimental kinetics as a ratio of areas under the profiles of the delayed and prompt kinetic components.

The above-mentioned kinetic model is expressed in terms of two coupled first-order linear differential equations with five rate constants corresponding to ISC ( $k_{ISC}$ ), RISC ( $k_{RISC}$ ), radiative ( $k_r^S$ ) and nonradiative ( $k_{IC}^S$ ) relaxations for  $S_1 \rightarrow S_0$ , as well as to the sum of the phosphorescence and nonradiative relaxation rate constants ( $k^T = k_r^T + k_{IC}^T$ ) for the  $T_1 \rightarrow S_0$  transition (Figure 1). Moreover, as long as the ISC and RISC processes are cyclic in nature ( $S_1 \rightarrow T_1 \rightarrow S_1 \rightarrow \dots$ , Figure 1) with excitation energy leakage in each cycle from  $S_1$  at the rate  $k_r^S + k_{IC}^S$  and from  $T_1$  at the rate  $k^T$ , then  $\Phi_p$  and  $\Phi_d$  are related to ISC QY ( $\Phi_{ISC}$ ) and RISC QY ( $\Phi_{RISC}$ ) as follows:  $\Phi_d + \Phi_p = \Phi_p / (1 - \Phi_{ISC}\Phi_{RISC})$  [111]. Considering that  $k_r^S$  can be found from a definition of the prompt FLQY,  $\Phi_p = k_r^S \tau_p$ , by experimental measurement of  $\Phi_p$  and  $\tau_p$ , whereas QYs of all the processes are determined by the corresponding rate constants, there are only four equations available for calculation of the five above-mentioned rates. Therefore, in general, one can unambiguously find all the rate constants from the experimental FL kinetics and FLQY only using additional assumptions. In particular, for the most efficient luminophores, for example, those with  $\Phi_p > 90\text{--}95\%$ , internal conversion contribution to the  $S_1 \rightarrow S_0$  transition is ignored, i.e.  $k_{IC}^S = 0$  is assumed [109,112]. Also in some cases, the relaxation  $T_1 \rightarrow S_0$  is ignored, i.e.  $k^T = 0$  is assumed [7,109], also implying  $\Phi_{RISC} = 1$ , which is probably not always sufficiently justified. To completely determine all the kinetic model parameters, one could also measure the phosphorescence lifetime ( $1/k^T$ ), however, such data for the MRTADF luminophores is usually not reported, which may be due to very weak phosphorescence intensity.

Note that RISC in some MRTADF luminophores probably occurs via higher triplet states  $T_n$  ( $n = 2, 3, \dots$ ), see the section below. Therefore, the three-level model may potentially become inadequate, so that, for example, a four-level model should be used instead [109]. However, the latter contains more unknown parameters than the three-level model does, which reduces the potential of the four-level model for experimental data interpretation.

### $\Delta E_{ST}$ gap

$\Delta E_{ST}$  is one of the key factors that determine the value of  $k_{RISC}$ , therefore, efficient TADF luminophores are sought for among molecules with the narrowest  $\Delta E_{ST}$  gap possible. The gap, in turn, can be extracted from the experimental

data using two following methods. The first method involves recording of the FL and phosphorescence spectra of a luminophore in solution or in an appropriate host and identifying the energy shift between the two spectra [26]. This can usually be achieved for MR luminophores at low temperatures (usually liquid nitrogen). Alternatively, the temperature dependence of the FL intensity can be measured, and its approximation by  $\exp(-\Delta E_{ST}/k_B T)$  can then be used to find  $\Delta E_{ST}$  [9]. In some cases, the two methods give different values of  $\Delta E_{ST}$ . In particular, for *v-DABNA*, the second method gives a considerably higher  $\Delta E_{ST}$  (70 meV) than the first one does (17 meV), which is attributed to the involvement of higher triplet states ( $T_1, T_2$ , etc.) in RISC [26] due to the spin-vibronic coupling.

In principle,  $\Delta E_{ST}$  can be derived from quantum chemical calculations, which is particularly valuable for molecular design of the TADF luminophores, however, the most widely used density functional theory calculations provide quite unreliable estimates in the case of small gaps  $\Delta E_{ST} < 1$  eV, which depend considerably on the functional used [113–115]. Therefore, predictive power of  $\Delta E_{ST}$  calculations using density functional theory methods and, especially, using semi-empirical methods is quite limited. On the other hand, *ab initio* methods such as the coupled cluster method give much more accurate results [116], however, these methods demand a lot of computational resources, and their capabilities are significantly limited by the number of luminophore atoms, so that *DABNA-1*-sized molecules can hardly be calculated accurately using such methods.

The small  $\Delta E_{ST}$  gap is an important, but not the only parameter defining  $k_{RISC}$ . This is illustrated in Figure 6 showing a correlation between  $k_{RISC}$  and  $\Delta E_{ST}$  plotted from the experimental data on the positions of FL and phosphorescence spectra as described above. As follows from this figure,  $k_{RISC}$  generally grows as  $\Delta E_{ST}$  decreases, however, the degree of correlation of these two values is quite modest. Such a low degree of correlation may be related to the following factors. First, effective involvement of higher triplet states in RISC is possible, for which the exponent should contain the gap  $E(T_n) - E(T_1)$ , where  $n = 1, 2, \dots$  is the number of the triplet excited state involved in the RISC process. This is indicated by a series of studies where, despite a relatively small  $\Delta E_{ST}$ , the rate  $k_{RISC}$  is moderately low (Figure 6), see, for example, [80,117–120]. In fact, as mentioned above, the matrix element of the spin-orbit coupling between the *S*- and *T*-states with the same electronic configuration, for example,  $\langle S_1 | \hat{H}_{SO} | T_1 \rangle$  or  $\langle S_3 | \hat{H}_{SO} | T_3 \rangle$ , should be small in the Condon approximation according to the El-Sayed rule [105]. Second, the value of  $\langle S_1 | \hat{H}_{SO} | T_1 \rangle$  can potentially strongly vary for different MR luminophores. Finally,  $k_{RISC}$  may be determined inaccurately from the experimental data due to the assumptions concerning  $k_{IC}^S$  and/or  $k^T$  (see above). Note that the highest values of  $k_{RISC}$  were reported for the MRTADF luminophores with heavy atoms (Figure 6, black dots), which is quite expected.

## TADF OLED stability

One of the severe disadvantages of TADF OLEDs is their insufficient operational stability in working conditions, especially for blue and shorter-wavelength OLEDs, and increasing the stability is one of the important problems to be solved [11]. The published research on the TADF OLED operational stability is very insufficient and incomplete, which is probably associated with the following circumstances. First, the data on low-stability OLED samples is probably often not published for „marketing“ reasons, not to reduce the publication potential of the results obtained. Moreover, it is highly likely that results for more stable TADF luminophores are not published, but are rather withheld for further patenting and commercialization. Second, the OLED operational stability parameters depend considerably not only on the TADF luminophore itself, but also on a set of other OLED parameters and measurement conditions, in particular, on the device architecture, utilization of additional layers, availability and quality of OLED sealing, on the atmosphere (inert gas vs. natural atmosphere, temperature, etc.) [11]. These parameters and conditions are often much different in publications of various research teams, which significantly hinders the comparison of operational stability results. Third, to improve the OLED operational stability, it is of prime importance to identify the mechanisms of OLED degradation [123], which requires targeted photo/electrophysical and EL studies supported by device physics simulations, for example, using drift-diffusion models. There is very little amount of such research on TADF OLED, but these studies are very important, allowing one to identify the key „culprits“ responsible for OLED degradation, namely, various excited states including singlet, triplet and/or polaron states. For example, the efficiency roll-off with an increase in current is often associated with the triplet-triplet annihilation, while the triplet-polaron annihilation may be responsible for irreversible degradation [124]. The OLED operational stability is usually measured by the time of roll-off down to 50% of the initial brightness (LT50), with 1000 cd/m<sup>2</sup> usually taken for the latter. The first MRTADF OLED versions on *DABNA-I* and its derivative *t-DABNA* showed very short operation lifetimes LT50 = 36.5 and 135 h at 1000 cd/m<sup>2</sup>, respectively, [11] (recalculation to LT50 at a reference brightness of 1000 cd/m<sup>2</sup> was performed using a procedure from [125]). Attempts were also made to use MRTADF as a terminal emitter in the emitting OLED layer as, for example, in [126], where *t-Bu-v-DABNA* as a terminal emitter for *pMDBA-DI* showed LT50 = 440 h at 1000 cd/m<sup>2</sup>. According to [127], the longest operational lifetime among MRTADF OLEDs is demonstrated by the OLED based on the *DBA-DI* luminophore in a mixed *mCBP-CN:DDBFT* host, for which LT50 = 540 h at 1000 cd/m<sup>2</sup> was reported.

## Conclusion

Thus, the analysis of the literature data shows that the key „bottlenecks“ of the 3rd-generation OLEDs are the wide EL band, leading to a reduced color purity, and the insufficient operational stability. At the same time, the MRTADF luminophores, in particular, of the *DABNA* class, appear to be one of the most promising types of materials for the 3rd-generation OLEDs. Though these luminophores exhibit high EL efficiency, increase in the TADF OLED operational lifetime and brightness is a complicated and important problem requiring identification of the correlation between the luminophore/host molecular structures and the photo/electrophysical and EL properties, both for the isolated luminophore and the one in the host, or in the luminophore neat film, where interactions of host/luminophore excitons and charges with various excited states are important. It appears that the most promising approach to the search for TADF luminophores that are most suitable for OLED technologies is in a combination of theoretical calculations of the molecular structure and electronic properties at the isolated-molecule level, detailed experimental and theoretical studies of photophysical processes, primarily using luminescence spectroscopy, and OLED simulations using drift-diffusion models accounting for the behavior of excitons of various multiplicities.

## Acknowledgments

The authors thank N.O. Dubinets and A.Yu. Sosorev for fruitful discussions.

## Funding

This study was supported by the Russian Science Foundation within grant No. 24-49-02038.

## Conflict of interest

The authors declare that they have no conflict of interest.

## References

- [1] V.M. Agranovich. *Theory of excitons* (Nauka, Moscow, 1968).
- [2] T. Hatakeyama, K. Shiren, K. Nakajima, S. Nomura, S. Nakatsuka, K. Kinoshita, J. Ni, Y. Ono, T. Ikuta. *Adv. Mater.*, **28** (14), 2777 (2016). DOI: 10.1002/adma.201505491
- [3] S. Madayanad Suresh, D. Hall, D. Beljonne, Y. Olivier, E. Zysman-Colman. *Adv. Funct. Mater.*, **30** (33), 1908677 (2020). DOI: 10.1002/adfm.201908677
- [4] H.J. Kim, T. Yasuda. *Adv. Opt. Mater.*, **10** (22), 2201714 (2022). DOI: 10.1002/adom.202201714
- [5] M. Mamada, M. Hayakawa, J. Ochi, T. Hatakeyama. *Chem. Soc. Rev.*, **53** (3), 1624 (2024). DOI: 10.1039/D3CS00837A
- [6] M. Furno, R. Meerheim, S. Hofmann, B. L sem, K. Leo. *Phys. Rev. B*, **85** (11), 115205 (2012). DOI: 10.1103/PhysRevB.85.115205

- [7] H. Kaji, H. Suzuki, T. Fukushima, K. Shizu, K. Suzuki, S. Kubo, T. Komino, H. Oiwa, F. Suzuki, A. Wakamiya, Y. Murata, C. Adachi. *Nat. Commun.*, **6** (1), 8476 (2015). DOI: 10.1038/ncomms9476
- [8] H. Yersin, L. Mataranga-Popa, R. Czerwieniec, Y. Dovbii. *Chem. Mat.*, **31** (16), 6110 (2019). DOI: 10.1021/acs.chemmater.9b01168
- [9] H. Uoyama, K. Goushi, K. Shizu, H. Nomura, C. Adachi. *Nature*, **492** (7428), 234 (2012). DOI: 10.1038/nature11687
- [10] O. Sachnik, Y. Li, X. Tan, J.J. Michels, P.W.M. Blom, G.-J.A.H. Wetzelaer. *Adv. Mater.*, **35** (26), e2300574 (2023). DOI: 10.1002/adma.202300574
- [11] E. Tankelevičiūtė, I.D.W. Samuel, E. Zysman-Colman. *J. Phys. Chem. Lett.*, **15** (4), 1034 (2024). DOI: 10.1021/acs.jpcclett.3c03317
- [12] H. Nakanotani, T. Higuchi, T. Furukawa, K. Masui, K. Morimoto, M. Numata, H. Tanaka, Y. Sagara, T. Yasuda, C. Adachi. *Nat. Commun.*, **5** (1), 4016 (2014). DOI: 10.1038/ncomms5016
- [13] N. Aizawa, Y.-J. Pu, Y. Harabuchi, A. Nihonyanagi, R. Ibuka, H. Inuzuka, B. Dhara, Y. Koyama, K.I. Nakayama, S. Maeda, F. Araoka, D. Miyajima. *Nature*, **609** (7927), 502 (2022). DOI: 10.1038/s41586-022-05132-y
- [14] Y. Lee, J. Kim, S. Lee, E. Sim, J.-I. Hong. *Chem. Eng. J.*, **476** 146659 (2023). DOI: 10.1016/j.ccej.2023.146659
- [15] R. Pollice, P. Friederich, C. Lavigne, G.d.P. Gomes, A. Aspuru-Guzik. *Matter*, **4** (5), 1654 (2021). DOI: 10.1016/j.matt.2021.02.017
- [16] R. Pollice, B. Ding, A. Aspuru-Guzik. *Matter*, **7** (3), 1161 (2024). DOI: 10.1016/j.matt.2024.01.002
- [17] S. Shao, J. Hu, X. Wang, L. Wang, X. Jing, F. Wang. *J. Am. Chem. Soc.*, **139** (49), 17739 (2017). DOI: 10.1021/jacs.7b10257
- [18] S. Shao, L. Wang. *Aggregate*, **1** (1), 45 (2020). DOI: 10.1002/agt2.4
- [19] X. Lv, Y. Wang, N. Li, X. Cao, G. Xie, H. Huang, C. Zhong, L. Wang, C. Yang. *Chem. Eng. J.*, **402**, 126173 (2020). DOI: 10.1016/j.ccej.2020.126173
- [20] T. Huang, Q. Wang, G. Meng, L. Duan, D. Zhang. *Angew. Chem. Int. Ed.*, **61** (12), e202200059 (2022). DOI: 10.1002/anie.202200059
- [21] Z. Zhao, C. Zeng, X. Peng, Y. Liu, H. Zhao, L. Hua, S.-J. Su, S. Yan, Z. Ren. *Angew. Chem. Int. Ed.*, **61** (39), e202210864 (2022). DOI: 10.1002/anie.202210864
- [22] Q. Zheng, X.-Q. Wang, Y.-K. Qu, G. Xie, L.-S. Liao, Z.-Q. Jiang. *npj flex. electron.*, **6** (1), 83 (2022). DOI: 10.1038/s41528-022-00212-5
- [23] J. Liu, Z. Feng, C. Peng, Y. Yu, S. Yang, Z. Jiang, L. Liao. *Chin. Chem. Lett.*, **34** (6), 107634 (2023). DOI: 10.1016/j.ccllet.2022.06.057
- [24] M.Y. Wong, E. Zysman-Colman. *Adv. Mater.*, **29** (22), 1605444 (2017). DOI: 10.1002/adma.201605444
- [25] M.J.S. Dewar, R.C. Dougherty. *The PMO Theory of Organic Chemistry* (Springer US, 1975).
- [26] Y. Kondo, K. Yoshiura, S. Kitera, H. Nishi, S. Oda, H. Gotoh, Y. Sasada, M. Yanai, T. Hatakeyama. *Nat. Photonics*, **13** (10), 678 (2019). DOI: 10.1038/s41566-019-0476-5
- [27] I.S. Park, M. Yang, H. Shibata, N. Amanokura, T. Yasuda. *Adv. Mater.*, **34** (9), 2107951 (2022). DOI: 10.1002/adma.202107951
- [28] K. Rayappa Naveen, H. Lee, R. Braveenth, K. Joon Yang, S. Jae Hwang, J. Hyuk Kwon. *Chem. Eng. J.*, **432**, 134381 (2022). DOI: 10.1016/j.ccej.2021.134381
- [29] C.A. Coulson, J.E. Lennard-Jones. *Proc. R. soc. Lond. Ser. A-Contain. Pap. Math. Phys.*, **169** (938), 413 (1939). DOI: 10.1098/rspa.1939.0006
- [30] R. Keruckiene, A.A. Vaitusionak, M.I. Hulnik, I.A. Bereziako, D. Gudeika, S. Macionis, M. Mahmoudi, D. Volyniuk, D. Valverde, Y. Olivier, K.L. Woon, S.V. Kostjuk, S. Reineke, J.V. Grazulevicius, G. Sini. *J. Mater. Chem. C*, **12** (10), 3450 (2024). DOI: 10.1039/D3TC04397E
- [31] T.P. Kaloni, R.P. Joshi, N.P. Adhikari, U. Schwingenschlögl. *Appl. Phys. Lett.*, **104** (7), 073116 (2014). DOI: 10.1063/1.4866383
- [32] H. Li, S. Zhu, M. Zhang, P. Wu, J. Pang, W. Zhu, W. Jiang, H. Li. *ACS Omega*, **2** (9), 5385 (2017). DOI: 10.1021/acsomega.7b00795
- [33] S.H. Han, J.H. Jeong, J.W. Yoo, J.Y. Lee. *J. Mater. Chem. C*, **7** (10), 3082 (2019). DOI: 10.1039/C8TC06575F
- [34] H. Hirai, K. Nakajima, S. Nakatsuka, K. Shiren, J. Ni, S. Nomura, T. Ikuta, T. Hatakeyama. *Angew. Chem. Int. Ed.*, **54** (46), 13581 (2015). DOI: 10.1002/anie.201506335
- [35] Y. Yuan, X. Tang, X.-Y. Du, Y. Hu, Y.-J. Yu, Z.-Q. Jiang, L.-S. Liao, S.-T. Lee. *Adv. Opt. Mater.*, **7** (7), 1801536 (2019). DOI: 10.1002/adom.201801536
- [36] X. Li, Y.-Z. Shi, K. Wang, M. Zhang, C.-J. Zheng, D.-M. Sun, G.-L. Dai, X.-C. Fan, D. Q. Wang, W. Liu, Y.-Q. Li, J. Yu, X.-M. Ou, C. Adachi, X.-H. Zhang. *ACS Appl. Mater. Interfaces*, **11** (14), 13472 (2019). DOI: 10.1021/acsami.8b19635
- [37] R.K. Konidena, K.R. Naveen. *Adv. Photon. Res.*, **3** (11), 2200201 (2022). DOI: 10.1002/adpr.202200201
- [38] H.L. Lee, W.J. Chung, J.Y. Lee. *Small*, **16** (14), 1907569 (2020). DOI: 10.1002/sml.201907569
- [39] V.V. Patil, H.L. Lee, I. Kim, K.H. Lee, W.J. Chung, J. Kim, S. Park, H. Choi, W.-J. Son, S.O. Jeon, J.Y. Lee. *Adv. Sci.*, **8** (20), 2101137 (2021). DOI: 10.1002/advs.202101137
- [40] G. Meng, D. Zhang, J. Wei, Y. Zhang, T. Huang, Z. Liu, C. Yin, X. Hong, X. Wang, X. Zeng, D. Yang, D. Ma, G. Li, L. Duan. *Chem. Sci.*, **13** (19), 5622 (2022). DOI: 10.1039/D2SC01543A
- [41] G. Meng, X. Chen, X. Wang, N. Wang, T. Peng, S. Wang. *Adv. Opt. Mater.*, **7** (11), 1900130 (2019). DOI: 10.1002/adom.201900130
- [42] Y. Lee, J.-I. Hong. *Adv. Opt. Mater.*, **9** (15), 2100406 (2021). DOI: 10.1002/adom.202100406
- [43] J. Wei, C. Zhang, D. Zhang, Y. Zhang, Z. Liu, Z. Li, G. Yu, L. Duan. *Angew. Chem. Int. Ed.*, **60** (22), 12269 (2021). DOI: 10.1002/anie.202017328
- [44] X. Cao, K. Pan, J. Miao, X. Lv, Z. Huang, F. Ni, X. Yin, Y. Wei, C. Yang. *J. Am. Chem. Soc.*, **144** (50), 22976 (2022). DOI: 10.1021/jacs.2c09543
- [45] H.-J. Cheon, S.-J. Woo, S.-H. Baek, J.-H. Lee, Y.-H. Kim. *Adv. Mater.*, **34** (50), 2207416 (2022). DOI: 10.1002/adma.202207416
- [46] T. Fan, Y. Zhang, L. Wang, Q. Wang, C. Yin, M. Du, X. Jia, G. Li, L. Duan. *Angew. Chem. Int. Ed.*, **61** (52), e202213585 (2022). DOI: 10.1002/anie.202213585
- [47] X. He, J. Lou, B. Li, H. Wang, X. Peng, G. Li, L. Liu, Y. Huang, N. Zheng, L. Xing, Y. Huo, D. Yang, D. Ma, Z. Zhao, Z. Wang, B.Z. Tang. *Angew. Chem. Int. Ed.*, **61** (48), e202209425 (2022). DOI: 10.1002/anie.202209425
- [48] H. Lee, R. Braveenth, J.D. Park, C.Y. Jeon, H.S. Lee, J.H. Kwon. *ACS Appl. Mater. Interfaces*, **14** (32), 36927 (2022). DOI: 10.1021/acsami.2c10127
- [49] Y.-T. Lee, C.-Y. Chan, M. Tanaka, M. Mamada, K. Goushi, X. Tang, Y. Tsuchiya, H. Nakanotani, C. Adachi. *Adv. Opt. Mater.*, **10** (17), 2200682 (2022).

- DOI: 10.1002/adom.202200682
- [50] J. Liu, L. Chen, X. Wang, Q. Yang, L. Zhao, C. Tong, S. Wang, S. Shao, L. Wang. *Macromol. Rapid Commun.*, **43** (16), 2200079 (2022). DOI: 10.1002/marc.202200079
- [51] T. Liu, C. Cheng, W. Lou, C. Deng, J. Liu, D. Wang, T. Tsuboi, Q. Zhang. *J. Mater. Chem. C*, **10** (20), 7799 (2022). DOI: 10.1039/D2TC00921H
- [52] X.-F. Luo, H.-X. Ni, A.-Q. Lv, X.-K. Yao, H.-L. Ma, Y.-X. Zheng. *Adv. Opt. Mater.*, **10** (16), 2200504 (2022). DOI: 10.1002/adom.202200504
- [53] J. Park, J. Moon, J. Lim, J. Woo, S.S. Yoon, J.Y. Lee. *J. Mater. Chem. C*, **10** (34), 12300 (2022). DOI: 10.1039/D2TC02283D
- [54] H.-J. Tan, G.-X. Yang, Y.-L. Deng, C. Cao, J.-H. Tan, Z.-L. Zhu, W.-C. Chen, Y. Xiong, J.-X. Jian, C. S. Lee, Q.-X. Tong. *Adv. Mater.*, **34** (18), 2200537 (2022). DOI: 10.1002/adma.202200537
- [55] S. Wu, A. Kumar Gupta, K. Yoshida, J. Gong, D. Hall, D.B. Cordes, A.M.Z. Slawin, I.D.W. Samuel, E. Zysman-Colman. *Angew. Chem. Int. Ed.*, **61** (52), e202213697 (2022). DOI: 10.1002/anie.202213697
- [56] C. Cao, J.-H. Tan, Z.-L. Zhu, J.-D. Lin, H.-J. Tan, H. Chen, Y. Yuan, M.-K. Tse, W. C. Chen, C.-S. Lee. *Angew. Chem. Int. Ed.*, **62** (10), e202215226 (2023). DOI: 10.1002/anie.202215226
- [57] Y. Chang, Y. Wu, X. Wang, W. Li, Q. Yang, S. Wang, S. Shao, L. Wang. *Chem. Eng. J.*, **451** (1), 138545 (2023). DOI: 10.1016/j.cej.2022.138545
- [58] G. Chen, J. Wang, W.-C. Chen, Y. Gong, N. Zhuang, H. Liang, L. Xing, Y. Liu, S. Ji, H. L. Zhang, Z. Zhao, Y. Huo, B.Z. Tang. *Adv. Funct. Mater.*, **33** (12), 2211893 (2023). DOI: 10.1002/adfm.202211893
- [59] H. Dai, J. Zhou, G. Meng, L. Wang, L. Duan, D. Zhang. *Chin. J. Chem.*, **41** (6), 657 (2023). DOI: 10.1002/cjoc.202200693
- [60] C.-Z. Du, Y. Lv, H. Dai, X. Hong, J. Zhou, J.-K. Li, R.-R. Gao, D. Zhang, L. Duan, X. Y. Wang. *J. Mater. Chem. C*, **11** (7), 2469 (2023). DOI: 10.1039/D2TC04952J
- [61] X.-C. Fan, F. Huang, H. Wu, H. Wang, Y.-C. Cheng, J. Yu, K. Wang, X.-H. Zhang. *Angew. Chem. Int. Ed.*, **62** (35), e202305580 (2023). DOI: 10.1002/anie.202305580
- [62] Y.-N. Hu, X.-C. Fan, F. Huang, Y.-Z. Shi, H. Wang, Y.-C. Cheng, M.-Y. Chen, K. Wang, J. Yu, X. H. Zhang. *Adv. Opt. Mater.*, **11** (3), 2202267 (2023). DOI: 10.1002/adom.202202267
- [63] Y. Hu, J. Miao, C. Zhong, Y. Zeng, S. Gong, X. Cao, X. Zhou, Y. Gu, C. Yang. *Angew. Chem. Int. Ed.*, **62** (19), e202302478 (2023). DOI: 10.1002/anie.202302478
- [64] Y. Hu, M. Huang, H. Liu, J. Miao, C. Yang. *Angew. Chem. Int. Ed.*, **62** (46), e202312666 (2023). DOI: 10.1002/anie.202312666
- [65] F. Huang, X.-C. Fan, Y.-C. Cheng, H. Wu, X. Xiong, J. Yu, K. Wang, X.-H. Zhang. *Angew. Chem. Int. Ed.*, **62** (32), e202306413 (2023). DOI: 10.1002/anie.202306413
- [66] Z. Huang, H. Xie, J. Miao, Y. Wei, Y. Zou, T. Hua, X. Cao, C. Yang. *J. Am. Chem. Soc.*, **145** (23), 12550 (2023). DOI: 10.1021/jacs.3c01267
- [67] J. Jin, C. Duan, H. Jiang, P. Tao, H. Xu, W.-Y. Wong. *Angew. Chem. Int. Ed.*, **62** (18), e202218947 (2023). DOI: 10.1002/anie.202218947
- [68] H.S. Kim, H.J. Cheon, D. Lee, W. Lee, J. Kim, Y.-H. Kim, S. Yoo. *Sci. Adv.*, **9** (22), eadfl388 (2023). DOI: doi:10.1126/sciadv.adfl388
- [69] X.-J. Liao, D. Pu, L. Yuan, J. Tong, S. Xing, Z.-L. Tu, J.-L. Zuo, W.-H. Zheng, Y. X. Zheng. *Angew. Chem. Int. Ed.*, **62** (6), e202217045 (2023). DOI: 10.1002/anie.202217045
- [70] B. Lei, Z. Huang, S. Li, J. Liu, Z. Bin, J. You. *Angew. Chem. Int. Ed.*, **62** (12), e202218405 (2023). DOI: 10.1002/anie.202218405
- [71] M. Luo, W. Li, L. Lyu, D. Li, S. Du, M. Zhao, Z. Wang, J. Zhang, Y. Li, Z. Ge. *Adv. Opt. Mater.*, **11** (2), 2202176 (2023). DOI: 10.1002/adom.202202176
- [72] S. Luo, J. Wang, N. Li, X.-F. Song, X. Wan, K. Li, C. Yang. *Angew. Chem. Int. Ed.*, **62** (49), e202310943 (2023). DOI: 10.1002/anie.202310943
- [73] S. Madayanad Suresh, L. Zhang, D. Hall, C. Si, G. Ricci, T. Matulaitis, A.M.Z. Slawin, S. Warriner, Y. Olivier, I.D.W. Samuel, E. Zysman-Colman. *Angew. Chem. Int. Ed.*, **62** (8), e202215522 (2023). DOI: 10.1002/anie.202215522
- [74] G. Meng, H. Dai, J. Zhou, T. Huang, X. Zeng, Q. Wang, X. Wang, Y. Zhang, T. Fan, D. Yang, D. Ma, D. Zhang, L. Duan. *Chem. Sci.*, **14** (4), 979 (2023). DOI: 10.1039/D2SC06343C
- [75] C. Qu, Y. Zhu, L. Liang, K. Ye, Y. Zhang, H. Zhang, Z. Zhang, L. Duan, Y. Wang. *Adv. Opt. Mater.*, **11** (8), 2203030 (2023). DOI: 10.1002/adom.202203030
- [76] E. Ravindran, H.E. Baek, H.W. Son, J.H. Park, Y.-H. Kim, M.C. Suh. *Adv. Funct. Mater.*, **33** (35), 2213461 (2023). DOI: 10.1002/adfm.202213461
- [77] Z. Wang, Z. Yan, Q. Chen, X. Song, J. Liang, K. Ye, Z. Zhang, H. Bi, Y. Wang. *ACS Appl. Mater. Interfaces*, **15** (11), 14605 (2023). DOI: 10.1021/acsami.2c23278
- [78] Y. Wang, R. Guo, A. Ying, K. Di, L. Chen, H. Gu, S. Liu, Y. Duan, H. Su, S. Gong, L. Wang. *Adv. Opt. Mater.*, **11** (1), 2202034 (2023). DOI: 10.1002/adom.202202034
- [79] K. Zhang, X. Wang, Y. Chang, Y. Wu, S. Wang, L. Wang. *Angew. Chem. Int. Ed.*, **62** (47), e202313084 (2023). DOI: 10.1002/anie.202313084
- [80] Y. Zou, M. Yu, J. Miao, T. Huang, S. Liao, X. Cao, C. Yang. *Chem. Sci.*, **14** (12), 3326 (2023). DOI: 10.1039/D3SC00246B
- [81] Y.-K. Chen, J. Lei, T.-L. Wu. *Chem. Sci.*, **15** (26), 10146 (2024). DOI: 10.1039/D4SC02351J
- [82] Y.-C. Cheng, X. Tang, K. Wang, X. Xiong, X.-C. Fan, S. Luo, R. Walia, Y. Xie, T. Zhang, D. Zhang, J. Yu, X.-K. Chen, C. Adachi, X.-H. Zhang. *Nat. Commun.*, **15** (1), 731 (2024). DOI: 10.1038/s41467-024-44981-1
- [83] W.-C. Guo, W.-L. Zhao, K.-K. Tan, M. Li, C.-F. Chen. *Angew. Chem. Int. Ed.*, **63** (18), e202401835 (2024). DOI: 10.1002/anie.202401835
- [84] X. Huang, J. Liu, Y. Xu, G. Chen, M. Huang, M. Yu, X. Lv, X. Yin, Y. Zou, J. Miao, X. Cao, C. Yang. *National Science Review*, **11** (6), nwa115 (2024). DOI: 10.1093/nsr/nwa115
- [85] H. Miranda-Salinas, J. Wang, A. Danos, T. Matulaitis, K. Stavrou, A.P. Monkman, E. Zysman-Colman. *J. Mater. Chem. C*, **12** (6), 1996 (2024). DOI: 10.1039/D3TC04394K
- [86] J. Ochi, Y. Yamasaki, K. Tanaka, Y. Kondo, K. Isayama, S. Oda, M. Kondo, T. Hatakeyama. *Nat. Commun.*, **15** (1), 2361 (2024). DOI: 10.1038/s41467-024-46619-8
- [87] Y. Qi, Z. Zhang, W. Sun, S. Wu, J. Liu, Z. Lin, P. Jiang, H. Yu, L. Zhou, G. Lu. *J. Mater. Chem. C*, **12** (17), 6319 (2024). DOI: 10.1039/D4TC00429A
- [88] R.W. Weerasinghe, J.M. dos Santos, Y. Chitose, T. Matulaitis, S.L. Warriner, D. Barman, C. Y. Chan, Y. Tsuchiya, E. Zysman-Colman, C. Adachi. *Phys. Chem. Chem. Phys.*, **26** (32), 21337 (2024). DOI: 10.1039/D4CP02664K

- [89] J. Xu, M. Wang, J. Chen, Z. Wu, T. Guo, B.Z. Tang, Z. Zhao. *Adv. Opt. Mater.*, **12** (23), 2400739 (2024). DOI: 10.1002/adom.202400739
- [90] L. Yuan, J.-W. Xu, Z.-P. Yan, Y.-F. Yang, D. Mao, J.-J. Hu, H.-X. Ni, C.-H. Li, J.-L. Zuo, Y.-X. Zheng. *Angew. Chem. Int. Ed.*, **63** (32), e202407277 (2024). DOI: 10.1002/anie.202407277
- [91] T.-Y. Zhang, Y.-C. Cheng, H. Wang, F. Huang, X. Xiong, X.-C. Fan, J. Yu, K. Wang, X. H. Zhang. *J. Mater. Chem. C*, **12** (15), 5386 (2024). DOI: 10.1039/D3TC04771G
- [92] Y. Zou, M. Yu, Y. Xu, Z. Xiao, X. Song, Y. Hu, Z. Xu, C. Zhong, J. He, X. Cao, K. Li, J. Miao, C. Yang. *Chem.*, **10** (5), 1485 (2024). DOI: 10.1016/j.chempr.2024.01.018
- [93] J. Park, K.J. Kim, J. Lim, T. Kim, J.Y. Lee. *Adv. Mater.*, **34** (21), 2108581 (2022). DOI: 10.1002/adma.202108581
- [94] S. Oda, B. Kawakami, R. Kawasumi, R. Okita, T. Hatakeyama. *Org. Lett.*, **21** (23), 9311 (2019). DOI: 10.1021/acs.orglett.9b03342
- [95] X. Liang, Z.-P. Yan, H.-B. Han, Z.-G. Wu, Y.-X. Zheng, H. Meng, J.-L. Zuo, W. Huang. *Angew. Chem. Int. Ed.*, **57** (35), 11316 (2018). DOI: 10.1002/anie.201806323
- [96] K. Matsui, S. Oda, K. Yoshiura, K. Nakajima, N. Yasuda, T. Hatakeyama. *J. Am. Chem. Soc.*, **140** (4), 1195 (2018). DOI: 10.1021/jacs.7b10578
- [97] F. Huang, K. Wang, Y.-Z. Shi, X.-C. Fan, X. Zhang, J. Yu, C.-S. Lee, X.-H. Zhang. *ACS Appl. Mater. Interfaces*, **13** (30), 36089 (2021). DOI: 10.1021/acsami.1c09743
- [98] Y. Zhang, D. Zhang, T. Huang, A.J. Gillett, Y. Liu, D. Hu, L. Cui, Z. Bin, G. Li, J. Wei, L. Duan. *Angew. Chem. Int. Ed.*, **60** (37), 20498 (2021). DOI: 10.1002/anie.202107848
- [99] P.K. Samanta, D. Kim, V. Coropceanu, J.-L. Brédas. *J. Am. Chem. Soc.*, **139** (11), 4042 (2017). DOI: 10.1021/jacs.6b12124
- [100] X.-K. Chen, D. Kim, J.-L. Brédas. *Acc. Chem. Res.*, **51** (9), 2215 (2018). DOI: 10.1021/acs.accounts.8b00174
- [101] T.J. Penfold, E. Gindensperger, C. Daniel, C.M. Marian. *Chem. Rev.*, **118** (15), 6975 (2018). DOI: 10.1021/acs.chemrev.7b00617
- [102] M. Hagai, N. Inai, T. Yasuda, K.J. Fujimoto, T. Yanai. *Sci. Adv.*, **10** (5), eadk3219 (2024). DOI: 10.1126/sciadv.adk3219
- [103] D.S. McClure. *J. Chem. Phys.*, **20** (4), 682 (1952). DOI: 10.1063/1.1700516
- [104] S.P. McGlynn, T. Azumi, M. Kinoshita. *Molecular Spectroscopy of the Triplet State* (Prentice-Hall, 1969).
- [105] M.A. El'Sayed. *J. Chem. Phys.*, **38** (12), 2834 (1963). DOI: 10.1063/1.1733610
- [106] D.S. McClure. *J. Chem. Phys.*, **17** (7), 665 (1949). DOI: 10.1063/1.1747359
- [107] V.M. Komarov, V.G. Plotnikov, L.V. Belousova. *Opt. Spectrosc.*, **29** (5), 533 (1970).
- [108] V.G. Plotnikov. *Russ. Chem. Rev.*, **49** (2), 172 (1980). DOI: 10.1070/RC1980v049n02ABEH002452
- [109] Y. Tsuchiya, S. Dising, F. Bencheikh, Y. Wada, P.L. dos Santos, H. Kaji, E. Zysman-Colman, I.D.W. Samuel, C. Adachi. *J. Phys. Chem. A*, **125** (36), 8074 (2021). DOI: 10.1021/acs.jpca.1c04056
- [110] J. Liu, Y. Zhu, T. Tsuboi, C. Deng, W. Lou, D. Wang, T. Liu, Q. Zhang. *Nat. Commun.*, **13** (1), 4876 (2022). DOI: 10.1038/s41467-022-32607-3
- [111] C. Baleizão, M.N. Berberan-Santos. *J. Chem. Phys.*, **126** (20), 204510 (2007). DOI: 10.1063/1.2734974
- [112] K. Masui, H. Nakanotani, C. Adachi. *Org. Electron.*, **14** (11), 2721 (2013). DOI: 10.1016/j.orgel.2013.07.010
- [113] T. Froitzheim, S. Grimme, J.-M. Mewes. *J. Chem. Theory Comput.*, **18** (12), 7702 (2022). DOI: 10.1021/acs.jctc.2c00905
- [114] M. Kondo. *Chem. Phys. Lett.*, **804**, 139895 (2022). DOI: 10.1016/j.cplett.2022.139895
- [115] J. Liang, X. Feng, D. Hait, M. Head-Gordon. *J. Chem. Theory Comput.*, **18** (6), 3460 (2022). DOI: 10.1021/acs.jctc.2c00160
- [116] A. Pershin, D. Hall, V. Lemaire, J.-C. Sancho-Garcia, L. Muccioli, E. Zysman-Colman, D. Beljonne, Y. Olivier. *Nat. Commun.*, **10** (1), 597 (2019). DOI: 10.1038/s41467-019-08495-5
- [117] J. Bian, S. Chen, L. Qiu, N. Zhang, J. Zhang, C. Duan, C. Han, H. Xu. *Research*, **2022**, 9838120 (2022). DOI: 10.34133/2022/9838120
- [118] J. Bian, S. Chen, L. Qiu, R. Tian, Y. Man, Y. Wang, S. Chen, J. Zhang, C. Duan, C. Han, H. Xu. *Adv. Mater.*, **34** (17), 2110547 (2022). DOI: 10.1002/adma.202110547
- [119] H. Chen, T. Fan, G. Zhao, D. Zhang, G. Li, W. Jiang, L. Duan, Y. Zhang. *Angew. Chem. Int. Ed.*, **62** (20), e202300934 (2023). DOI: 10.1002/anie.202300934
- [120] Y. Sano, T. Shintani, M. Hayakawa, S. Oda, M. Kondo, T. Matsushita, T. Hatakeyama. *J. Am. Chem. Soc.*, **145** (21), 11504 (2023). DOI: 10.1021/jacs.3c02873
- [121] Y. Xu, Q. Wang, X. Cai, C. Li, Y. Wang. *Adv. Mater.*, **33** (21), 2100652 (2021). DOI: 10.1002/adma.202100652
- [122] Y. Yang, N. Li, J. Miao, X. Cao, A. Ying, K. Pan, X. Lv, F. Ni, Z. Huang, S. Gong, C. Yang. *Angew. Chem. Int. Ed.*, **61** (30), e202202227 (2022). DOI: 10.1002/anie.202202227
- [123] J. Jiang, J.Y. Lee. *Mater. Today*, **68**, 204 (2023). DOI: 10.1016/j.mattod.2023.06.016
- [124] B. van der Zee, Y. Li, G.-J.A.H. Wetzelaer, P.W.M. Blom. *Phys. Rev. Appl.*, **18** (6), 064002 (2022). DOI: 10.1103/PhysRevApplied.18.064002
- [125] W. Zhang, Z. Wu, S. Liang, B. Jiao, X. Zhang, D. Wang, X. Hou, Z. Chen, Q. Gong. *J. Phys. D: Appl. Phys.*, **44** (15), 155103 (2011). DOI: 10.1088/0022-3727/44/15/155103
- [126] K.R. Naveen, H. Lee, R. Braveenth, D. Karthik, K.J. Yang, S.J. Hwang, J.H. Kwon. *Adv. Funct. Mater.*, **32** (12), 2110356 (2022). DOI: 10.1002/adfm.202110356
- [127] D.H. Ahn, J.H. Maeng, H. Lee, H. Yoo, R. Lampande, J.Y. Lee, J.H. Kwon. *Adv. Opt. Mater.*, **8** (11), 2000102 (2020). DOI: 10.1002/adom.202000102

Translated by E. Ilinskaya